Polarizabilities of the Mg^+ and Si^{3+} ions

J. Mitroy
School of Engineering, Charles Darwin University, Darwin NT 0909, Australia

M. S. Safronova
Department of Physics and Astronomy, University of Delaware, Newark, Delaware 19716-2593, USA

(Received 2 November 2008; published 29 January 2009)

A polarization analysis of the fine-structure intervals for the $n=17$ Rydberg states of Mg and the $n=29$ states of Si^{2+} is performed. The coefficients of all terms in the polarization expansion up to r^{-8} were computed using a semiempirical single electron analysis combined with the relativistic all-order single-double method (MBPT-SD) which includes all single-double excitations from the Dirac-Fock wave functions to all orders of perturbation theory. The revised analysis yields dipole polarizabilities of $\alpha_1=35.04(3)$ a.u. for Mg^+ and $\alpha_1=7.433(25)$ a.u. for Si^{3+}, values only marginally larger than those obtained in a previous analysis [E. L. Snow and S. R. Lundeen, Phys. Rev. A **75**, 062512 (2007); **77**, 052501 (2008)]. The polarizabilities are used to make estimates of the multiplet strength for the resonant transition for both ions. The revised analysis did see significant changes in the slopes of the polarization plots. The dipole polarizabilities from the MBPT-SD calculation, namely 35.05(12) a.u. and 7.419(16) a.u., are within 0.3% of the revised experimental values.

DOI: 10.1103/PhysRevA.79.012513 PACS number(s): 31.15.ap, 31.15.ag, 31.15.am, 31.15.V−

I. INTRODUCTION

Resonant excitation Stark ionization spectroscopy (RESIS) [1] is a versatile and powerful method for studying Rydberg states of atoms and ions. One of the primary applications is the determination of deviations from the pure hydrogenic values of the binding energies. Polarization interactions between the core and the Rydberg electrons lead to the effective potential [1–3]

$$V_{\rm pol}=-\frac{C_4}{r^4}-\frac{C_6}{r^6}-\frac{C_7}{r^7}-\frac{C_8}{r^8}-\frac{C_{8L}L(L+1)}{r^8}+\cdots . \quad (1)$$

The leading-order term is directly related to the static dipole polarizability by the identity $C_4=\alpha_1/2$. The next term C_6 is related to the quadrupole polarizability, α_2, and nonadiabatic dipole polarizability, β_1, through the relation $C_6=(\alpha_2-6\beta_1)/2$. Equation (1) had been used as a cornerstone in the analysis of the RESIS fine-structure spectrum of the Rydberg states of neutral Mg and Si^{2+}. This resulted in precise estimates of the dipole polarizabilities of the Mg^+ and Si^{3+} ground states [4–6]. Both of these ions are sodiumlike with one valence electron orbiting the nucleus and the ten tightly bound core electrons. The Mg^+ dipole polarizability was 35.00(5) a.u. [6] and the Si^{3+} dipole polarizability was 7.426(12) a.u. [5]. Analysis of these spectra has also given information about the quadrupole polarizabilities.

Investigations into atomic polarizabilities have implications that go beyond describing the response of the electron charge distribution to the presence of an external electric field. One of the most active areas in physics at present is the development of new atomic clocks based on groups of neutral atoms in optical lattices [7–9] or single atomic ions [7,10]. These clocks have the potential to exceed the precision of the existing cesium microwave standard [11]. For many of these clocks the single largest source of systematic error is the blackbody radiation shift (BBR) [12–16]. The BBR shift to first order is proportional to the difference in polarizabilities of the two states involved in the clock transition. Many estimates of the relevant polarizabilities are determined by theoretical calculations [17–19]. Comparisons of existing techniques to calculate polarizabilities with high quality experiments will ultimately help constrain the uncertainties associated with the BBR shift.

One area of uncertainty in the RESIS analysis is the contribution of the higher-order terms in the polarization expansion. The desirable outcomes of a RESIS experiment are the determination of C_4 and C_6. However, extracting precise values of C_4 and C_6 from the fine-structure spectrum is reliant upon having reasonable estimates of the higher-order polarization constants, namely C_7, C_8, and C_{8L}. This is particularly important in the case of C_6. Analyses of the fine-structure intervals that omit the higher-order polarization potentials yield values of C_6 and α_2 that are quite different from estimates from atomic structure theories [4–6]. Unfortunately, the best analyses of RESIS data so far have not had a complete description of all the individual terms that contribute to C_7, C_8, and C_{8L}. While the omission of some of the higher-order polarizabilities would only be expected to have a minor influence on C_4, the possible impact on the derived quadrupole polarizability is unknown and could easily be of order 50%.

The present paper presents a theoretical analysis of the polarizabilities of the Mg^+ and Si^{3+} ions. The purpose of this analysis is twofold. First, comparison with RESIS derived dipole and quadrupole polarizabilities gives a stringent test of the ability of atomic structure theories to correct predict these polarizabilities for sodiumlike atoms. Second, all the higher-order polarizabilities contributing to C_7, C_8, and C_{8L} were explicitly calculated. This permitted a more refined analysis of the RESIS data. The reevaluation of the RESIS experimental data gave dipole polarizabilities that were marginally largely than previously published values [5,6] and quadrupole polarizabilities that were markedly different from previously published values [5,6].

II. THE POLARIZATION EXPANSION

In this section the definitions of the various terms in the polarization potential are given following the analysis of Drachman [2,3]. The notation of Lundeen [1,5] is adopted.

The leading term, C_4, is half the size of the static dipole polarizability,

$$C_4 = \frac{\alpha_1}{2}. \tag{2}$$

The dipole polarizability is defined as

$$\alpha_1 = \sum_n \frac{f_{gn}^{(1)}}{(\Delta E_{gn})^2}, \tag{3}$$

where $f_{gn}^{(k)}$ is the absorption oscillator strength for a dipole transition from state g to state n. The absorption oscillator strength for a multipole transition from $g \rightarrow n$, with an energy difference of $\Delta E_{ng} = E_g - E_n$ is defined as

$$f_{gn}^{(k)} = \frac{2|\langle \psi_g; L_g \| r^k \mathbf{C}^k(\hat{\mathbf{r}}) \| \psi_n; L_n \rangle|^2 \Delta E_{ng}}{(2k+1)(2L_g+1)}. \tag{4}$$

In this expression, L_g is the orbital angular momentum of the initial state while k is the polarity of the transition. In a J representation, the oscillator strength becomes

$$f_{gn}^{(k)} = \frac{2|\langle \psi_g; J_g \| r^k \mathbf{C}^k(\hat{\mathbf{r}}) \| \psi_n; J_n \rangle|^2 \Delta E_{ng}}{(2k+1)(2J_g+1)}. \tag{5}$$

The next term, C_6, is composed of two separate terms,

$$C_6 = \frac{\alpha_2 - 6\beta_1}{2}. \tag{6}$$

The quadrupole polarizability α_2 is computed as

$$\alpha_2 = \sum \frac{f_{gn}^{(2)}}{(\Delta E_{gn})^2}. \tag{7}$$

The second term in Eq. (6) is the nonadiabatic dipole polarizability. It is defined as

$$\beta_1 = \sum \frac{f_{gn}^{(1)}}{2(\Delta E_{gn})^3}. \tag{8}$$

The r^{-7} term, C_7, also comes in two parts, namely,

$$C_7 = -\frac{(\alpha_{112} + 3.2q\gamma_1)}{2}. \tag{9}$$

The γ_1 is a higher-order nonadiabatic term

$$\gamma_1 = \sum \frac{f_{gn}^{(1)}}{4(\Delta E_{gn})^4}, \tag{10}$$

while q is the charge on the core. The dipole-dipole-quadrupole polarizability, α_{112} arises from third order in perturbation theory. It is derived from the matrix element [2,5,20]

$$\frac{\alpha_{112}}{2R^7} = \sum_{k_1k_2k_3} \sum_{n_a n_b} \frac{\langle \psi_g; 0 | V^{k_1} | \psi_{n_a}; L_a \rangle}{\Delta E_{n_g n_a} \Delta E_{n_b n_a}} \times \langle \psi_{n_a}; L_a | V^{k_2} | \psi_{n_b}; L_b \rangle \times \langle \psi_{n_b}; L_b | V^{k_3} | \psi_g; 0 \rangle, \tag{11}$$

where $V^k = \mathbf{C}^k(\hat{\mathbf{r}}) \cdot \mathbf{C}^k(\hat{\mathbf{R}}) r^k / R^{K+1}$. The sum of the multipole orders must obey $k_1 + k_2 + k_3 = 4$. Quite a few terms contribute to C_8,

$$C_8 = \frac{\alpha_3 - \beta_2 - \alpha_1\beta_1 + \alpha_{1111} + 72\gamma_1}{2}. \tag{12}$$

The octupole polarizability, α_3, is computed as

$$\alpha_3 = \sum \frac{f_{gn}^{(3)}}{(\Delta E_{gn})^2}. \tag{13}$$

The β_2 comes from the nonadiabatic part of the quadrupole polarizability; it is

$$\beta_2 = \sum \frac{f_{gn}^{(2)}}{2(\Delta E_{gn})^3}. \tag{14}$$

The fourth-order term, α_{1111}, is related to the hyperpolarizability [21,22]. It is defined as

$$\frac{\alpha_{1111}}{2R^8} = \sum_{n_a n_b n_c} \frac{\langle \psi_{n_g}; 0 | V^1 | \psi_{n_a}; L_a \rangle}{\Delta E_{ga} \Delta E_{gb} \Delta E_{gc}} \langle \psi_{n_a}; L_a | V^1 | \psi_{n_b}; L_b \rangle \times \langle \psi_{n_b}; L_b | V^1 | \psi_{n_c}; L_c \rangle \langle \psi_{n_c}; L_c | V^1 | \psi_g; 0 \rangle. \tag{15}$$

The final term, C_{8L}, is nonadiabatic in origin and defined

$$C_{8L} = \frac{18\gamma_1}{5}. \tag{16}$$

III. STRUCTURE MODELS FOR Mg^+ AND Si^{3+}

The Mg^+ and Si^{3+} ions are sodiumlike systems that have one valence electron orbiting the ten electrons in the $1s^2 2s^2 2p^6$ core. Two different methods are used to determine the polarization response of these ions. One technique supplements the Hartree-Fock (HF) core potential with a semiempirical core polarization potential and effectively solves a one-electron Schrödinger equation to determine the excitation spectrum for the valence electron [23–25]. The other method used is the relativistic all-order single-double method where all single and double excitations of the Dirac-Fock (DF) wave function are included to all orders of many-body perturbation theory (MBPT) [26–28]. The agreement between the HF plus core polarization (HFCP) calculation and the MBPT calculation with single-double excitations (MBPT-SD) will be seen to be excellent.

We note in passing that there has also been a recent configuration interaction (CI) calculation of the polarizabilities of the Mg^+ and Si^{3+} ground states [29]. This CI calculation gave dipole polarizabilities which were slightly larger than the HFCP and MBPT-SD calculations. There has also been a relativistic coupled-cluster (RCC) calculation [30] of the Mg^+ polarizabilities.

A. Semiempirical method

The semiempirical wave functions and transition operator expectation values were computed by diagonalizing the semiempirical Hamiltonian [24,31–34] in a large mixed Laguerre-type orbital (LTO) and Slater-type orbital (STO) basis set [31]. We first discuss Si^{3+} and then mention Mg^+.

The initial step was to perform a HF calculation to define the core. The calculation of the Si^{3+} ground state was done in a STO basis [35]. The core wave functions were then frozen, giving the working Hamiltonian for the valence electron

$$H = -\frac{1}{2}\nabla^2 + V_{\rm dir}(\mathbf{r}) + V_{\rm exc}(\mathbf{r}) + V_{\rm p}(\mathbf{r}). \tag{17}$$

The direct and exchange interactions, $V_{\rm dir}$ and $V_{\rm exc}$, of the valence electron with the HF core were calculated exactly. The ℓ-dependent polarization potential, $V_{\rm p}$, was semiempirical in nature with the functional form

$$V_{\rm p}(\mathbf{r}) = -\sum_{\ell m} \frac{\alpha_d g_\ell^2(r)}{2r^4} |\ell m\rangle\langle \ell m|. \tag{18}$$

The coefficient, α_d, is the static dipole polarizability of the core and $g_\ell^2(r) = 1 - \exp(-r^6/\rho_\ell^6)$ is a cutoff function designed to make the polarization potential finite at the origin. The cutoff parameters, ρ_ℓ, were tuned to reproduce the binding energies of the *ns* ground state and the *np*, *nd*, and *nf* excited states. The energies of the states with $\ell \geqslant 1$ were tuned to the statistical average of their respective spin-orbit doublets. The dipole polarizability for Si^{4+} was chosen as $\alpha_d = 0.1624$ a.u. [31,36]. The cutoff parameters for $\ell = 0 \rightarrow 3$ were 0.7473, 0.8200, 1.022, and $0.900 a_0$, respectively. The parameters for $\ell > 3$ were set to ρ_3. The Hamiltonian was diagonalized in a very large orbital basis with about 50 LTOs for each ℓ value. The oscillator strengths (and other multipole expectation values) were computed with operators that included polarization corrections [31,32,37–39]. The quadrupole core polarizability was chosen as 0.1021 a.u. [36], while the octupole polarizability was set to zero. The cutoff parameter for the polarization correction to the transition operator was fixed at $0.864 a_0$ (the average of ρ_0, ρ_1, ρ_2, and ρ_3).

It is worth emphasizing that the model potential is based on a realistic wave function and the direct and exchange interactions with the core were computed without approximation from the HF wave function. Only the core polarization potential is described with an empirical potential.

The overall methodology of the Mg^+ calculation is the same as that for Si^{3+} and many of the details have been given previously [18]. The core polarizabilities were $\alpha_{1,\rm core} = 0.4814$ a.u. [23,31] and $\alpha_{2,\rm core} = 0.5183$ a.u. for Mg^{2+} [31,36]. The octupole polarizability was set to zero. The Mg^{2+} cutoff parameters for $\ell = 0 \rightarrow 3$ were 1.1795, 1.302, 1.442, and $1.520 a_0$, respectively. The cutoff parameter for evaluation of transition multipole matrix elements was $1.361 a_0$.

The HFCP calculations of the polarizabilities utilized the list of multipole matrix elements and energies resulting from the diagonalization of the effective Hamiltonian. These were directly used in the evaluation of the polarizability sum rules.

B. The all-order method

In the relativistic all-order method including single, double, and valence triple excitations, the wave function is represented as an expansion,

$$|\Psi_v\rangle = \left[1 + \sum_{ma} \rho_{ma} a_m^\dagger a_a + \frac{1}{2}\sum_{mnab} \rho_{mnab} a_m^\dagger a_n^\dagger a_b a_a + \sum_{m \neq v} \rho_{mv} a_m^\dagger a_v + \sum_{mna} \rho_{mnva} a_m^\dagger a_n^\dagger a_a a_v + \frac{1}{6}\sum_{mnrab} \rho_{mnrvab} a_m^\dagger a_n^\dagger a_r^\dagger a_b a_a a_v\right] |\Phi_v\rangle, \tag{19}$$

where Φ_v is the lowest-order atomic state wave function, which is taken to be the *frozen-core* DF wave function of a state v in our calculations. In second quantization, the lowest-order atomic state function is written as

$$|\Phi_v\rangle = a_v^\dagger |0_C\rangle,$$

where $|0_C\rangle$ represents the DF wave function of the closed core. In Eq. (19), $a_i^\dagger$ and a_i are creation and annihilation operators, respectively. Indices at the beginning of the alphabet, $a, b, \ldots$, refer to occupied core states, those in the middle of the alphabet $m, n, \ldots$, refer to excited states, and index v designates the valence orbital. We refer to ρ_{ma}, ρ_{mv} as single core and valence excitation coefficients and to ρ_{mnab} and ρ_{mnva} as double core and valence excitation coefficients, respectively. The quantities ρ_{mnrvab} are valence triple excitation coefficients and are included perturbatively where necessary as described in Ref. [27].

To derive the equations for the excitation coefficients, the wave function Ψ_v, given by Eq. (19), is substituted into the many-body Schrödinger equation

$$H|\Psi_v\rangle = E|\Psi_v\rangle, \tag{20}$$

where the Hamiltonian H is the relativistic *no-pair* Hamiltonian [40]. This can be expressed in second quantization as

$$H = \sum_i \epsilon_i :a_i^\dagger a_i: + \frac{1}{2}\sum_{ijkl} g_{ijkl} :a_i^\dagger a_j^\dagger a_l a_k:, \tag{21}$$

where ϵ_i is the DF energy for the state i, g_{ijkl} are the two-body Coulomb integrals, and $::$ indicates normal order of the operators with respect to the closed core. In the *no-pair* Hamiltonian, the contributions from negative-energy (positron) states are omitted.

The resulting all-order equations for the excitation coefficients ρ_{ma}, ρ_{mv}, ρ_{mnab}, and ρ_{mnva} are solved iteratively with a finite basis set, and the correlation energy is used as a convergence parameter. As a result, the series of correlation correction terms included in the SD (or SDpT) approach are included to all orders of MBPT as an additional MBPT order is picked up at each iteration. The basis set is defined in a spherical cavity on a nonlinear grid and consists of single-particle basis states which are linear combinations of B splines [41]. The contribution from the Breit interaction is negligible for all matrix elements considered in this work.

The matrix element of any one-body operator Z in the all-order method is obtained as

$$Z_{vw} = \frac{\langle \Psi_v | Z | \Psi_w \rangle}{\sqrt{\langle \Psi_v | \Psi_v \rangle \langle \Psi_w | \Psi_w \rangle}}. \quad (22)$$

The numerator of the resulting expression consists of the sum of the DF matrix element z_{wv} and twenty other terms $Z^{(k)}$, $k=a\cdots t$. These terms are linear or quadratic functions of the excitation coefficients ρ_{ma}, ρ_{mv}, ρ_{mnab}, and ρ_{mnva}. More details on the SD and SDpT methods and their applications can be found in Refs. [27,28,42]. We find that the contribution of triple excitations is small for the atomic properties considered in this work. So the SD approximation is used for most transitions.

The B-spline basis used in the calculations included $N=50$ basis orbitals for each angular momentum within a cavity radius of $R_0=100a_0$ for Mg^+ and $R_0=80a_0$ for Si^{3+}. Such large cavities are needed to fit highly excited states such as $8h$ needed for the $3d$ octupole polarizability calculations. The single-double (SD) all-order method yielded results for the primary ns-np_j electric-dipole matrix elements of alkali-metal atoms that are in agreement with experiment to 0.1%–0.5% [27]. We identify results obtained with this method as MBPT-SD in the subsequent text and tables.

Since the all-order calculations are carried out with a finite basis set, the sums given by Eqs. (3)–(13) run up to the number of the basis set orbitals ($N=50$) for each partial wave. For consistency, the same B-spline basis is used in all calculations of the same system (e.g., Mg^+ or Si^{3+}).

The calculation of the polarizabilities for the MBPT-SD uses slightly different procedures to include different parts of the polarizability sum rules. The all-order matrix elements were combined with the experimental energies for excited states with $n\leqslant 6$ for $\beta=ns,np_{1/2},np_{3/2},nd_{3/2},nd_{5/2}$, $n\leqslant 7$ for $\beta=nf_{5/2},nf_{7/2}$, and $n\leqslant 8$ for $\beta=ng_{7/2},ng_{9/2},nh_{9/2},nh_{11/2}$. The remaining matrix elements and energies were calculated in the DF approximation, with the exception of the $3s$ dipole polarizability, where the remaining matrix elements were calculated using the random-phase approximation (RPA) [43] for the purpose of error evaluation. These remainder contributions are small for dipole polarizabilities (0.2–5 %) but increase in relative size for the quadrupole (0.3–10 %) and octupole (4–20 %) polarizabilities. An extra correction was introduced to the remainder contribution for octupole polarizabilities. First, the accuracy of the DF calculations was estimated from a comparison of the DF and all-order results for the few first terms. Then, these estimates were used to adjust the remainder. The improvement of the DF results for states with higher n was also taken into account. The size of this extra correction ranged from 0.9% to 6% of the tail contributions as the accuracy of the DF approximation for these highly excited states is rather high. The net effect of this scaling was usually to reduce the octupole polarizabilities by an amount of about 0.5–1.5 %.

The core contribution was calculated in the RPA [36] with the exception of the dipole polarizability for the Mg^{2+} core. In this case the polarizability of $\alpha_d=0.4814$ a.u. was taken from a pseudonatural orbital CI type calculation [23,31]. A small α_{cv} correction for the dipole polarizability that compensates for excitations from the core to occupied valence states was also determined using RPA matrix elements and DF energies. The relative impact of the core polarizability was at least a factor of 2 smaller for the quadrupole polarizability.

TABLE I. Theoretical and experimental energy levels (in hartree) of some of the low-lying states of the Mg^+ and Si^{3+} ions. The energies are given relative to the energy of the Mg^{2+} and Sr^{4+} cores. The experimental energies are taken from the National Institute of Standards and Technology database [44]. The HFCP energies should be interpreted as the J weighted average of the spin-orbit doublet.

State	Experiment	MBPT-SD	HFCP
		Mg^+	
$3s_{1/2}$	−0.552536	−0.552522	−0.552536
$3p_{1/2}$	−0.390015	−0.390030	−0.389737
$3p_{3/2}$	−0.389597	−0.389611	
$4s_{1/2}$	−0.234481	−0.234470	−0.234323
$3d_{5/2}$	−0.226803	−0.226772	−0.226804
$3d_{3/2}$	−0.226799	−0.226768	
$4p_{1/2}$	−0.185206	−0.185210	−0.185014
$4p_{3/2}$	−0.185067	−0.185071	
$4d_{5/2}$	−0.127382	−0.127374	−0.127373
$4d_{3/2}$	−0.127379	−0.127372	
		Si^{3+}	
$3s_{1/2}$	−1.658930	−1.658973	−1.658928
$3p_{1/2}$	−1.334120	−1.334094	−1.332738
$3p_{3/2}$	−1.332019	−1.331999	
$3d_{5/2}$	−0.928210	−0.928138	−0.928302
$3d_{3/2}$	−0.928205	−0.928134	
$4s_{1/2}$	−0.775097	−0.775104	−0.774681
$4p_{1/2}$	−0.664433	−0.664421	−0.663640
$4p_{3/2}$	−0.663696	−0.663684	
$4d_{5/2}$	−0.519810	−0.519800	−0.519743
$4d_{3/2}$	−0.519809	−0.519799	
$4f_{5/2}$	−0.501044	−0.501044	−0.501033
$4f_{7/2}$	−0.501032	−0.501035	

IV. GROUND AND EXCITED PROPERTIES

A. The energy levels

The binding energies of the low-lying states of the Mg^+ and Si^{3+} are tabulated and compared with experiment in Table I. The agreement between the HFCP energies and the experimental energies is generally of order 10^{-4} hartree. When the ρ_ℓ cutoff parameters are tuned to the lowest state of each symmetry the tendency is for higher states of the same symmetry to be slightly underbound. The MBPT-SD binding energies generally agree with experiment to better than 10^{-4} hartree. The MBPT-SD binding energies do not exhibit any systematic tendency to either underbind or overbind as n increases.

B. Line strengths

Table II lists the line strengths for the resonant transitions of Na, Mg^+, Al^{2+}, and Si^{3+}. All line strengths here and in the

TABLE II. Line strengths (in a.u.) for the resonance transitions of Na, Mg^+, Al^{2+}, and Si^{3+}. Experimental values with citations are also given. The MBPT-SD results for Na and Al^{2+} are taken from [26].

Transition	HFCP	MBPT-SD	BSR-CI	Experiment
		Na		
$S^{(1)}_{3s\text{-}3p_{1/2}}$	12.44	12.47	12.60	12.412(16) [45,46]
				12.435(41) [47]
$S^{(1)}_{3s\text{-}3p_{3/2}}$	24.88	24.94	25.20	24.876(24) [48]
				24.818(34) [45,46]
				24.844(54) [49]
		Mg^+		
$S^{(1)}_{3s\text{-}3p_{1/2}}$	5.602	5.612	5.644	5.645(44) [50]
$S^{(1)}_{3s\text{-}3p_{3/2}}$	11.20	11.23	11.29	11.33(12) [50]
				11.24(6) [51]
		Al^{2+}		
$S^{(1)}_{3s\text{-}3p_{1/2}}$	3.398	3.404	3.422	3.01(29) [52]
				3.11(15) [53]
				3.31(35) [54]
$S^{(1)}_{3s\text{-}3p_{3/2}}$	6.796	6.817	6.851	6.02(57) [52]
				6.35(45) [53]
		Si^{3+}		
$S^{(1)}_{3s\text{-}3p_{1/2}}$	2.333	2.341	2.350	2.35(10) [55]
$S^{(1)}_{3s\text{-}3p_{3/2}}$	4.666	4.686	4.707	4.70(20) [55]

text below are given in a.u. The HFCP values for sodium are from calculations previously reported in Ref. [58] while the values for Al^{2+} were taken from a calculation very similar in style and execution to the present calculations [59]. The MBPT-SD line strengths for Na and Al^{2+} were taken from Ref. [26]. Values from the extensive tabulation of dipole line strengths using a *B*-spline nonorthogonal configuration interaction with the Breit interaction (BSR-CI) [60] are also listed. The HFCP line strengths were computed from a common multiplet strength by multiplying by the appropriate recoupling coefficients [61].

The comparisons for the resonant $3s \rightarrow 3p$ transition reveal that the HFCP line strengths are the smallest, the BSR-CI line strengths are the largest, and the MBPT-SD line strengths are intermediate between these two calculations. The MBPT-SD dipole strengths are closer to HFCP for Na, Mg^+, and Al^{2+} and about half-way between HFCP and BSR-CI for Si^{3+}. The total variation between the three different calculations is about 1%. The most precise experiments performed on the Na-like isoelectronic series of atoms (ions) are those performed on sodium itself [45–49]. The experimental line strengths for sodium are in better agreement with the MBPT-SD and HFCP line strengths than they are with the BSR-CI line strengths.

There have been two precision measurements of the $3s \rightarrow 3p$ transition rate for Mg^+. The experiment of Ansbacher *et al.* [50] gave slightly larger line strengths which agree best with the BSR-CI values. However, the most recent trapped ion experiment [51] gave a $3s_{1/2} \rightarrow 3p_{3/2}$ line strength of 11.24(6) that is in better agreement with the HFCP and MBPT-SD line strengths.

Table III lists the line strengths for a number of other dipole transitions for Mg^+ and Si^{3+}. The line strengths for the quadrupole $3s \rightarrow nd$ transitions are also listed due to their importance in the determination of the quadrupole polarizabilities.

The $3p \rightarrow 3d$ transition is the strongest transition emanating from the $3p$ level. The comparison between the three calculations exhibits a pattern similar to that of the resonant transition. The HFCP line strengths are smallest, the BSR-CI line strengths are the largest, and the MBPT-SD line strengths lie somewhere between these two calculations.

The astrophysically important Mg^+ $3s \rightarrow 4p$ transition has a very small dipole strength. It is close to the Cooper minimum [62] in the $3s \rightarrow np$ matrix elements and therefore is more sensitive to the slightly different energies between the spin-orbit doublet. This caused the ratio of line strengths for the $4p_{1/2}$ and $4p_{3/2}$ transitions to deviate from the expected value of 2. The MBPT-SD branching ratio of 1.76 agrees with the recent experimental values of 1.74(6) [63] and 1.82(8) [63,64]. The HFCP multiplet strength of 0.00752 and the MBPT-SD multiplet strength of 0.00721 are about 5–10 % smaller than the recent experimental estimates of 0.007 93(26) [63] and 0.007 75(50) [63,64].

There is also a deviation from the ratio of 2 for the $3s \rightarrow 4p_{1/2,3/2}$ transitions of Si^{3+}. However, in this case the deviation is smaller. Ratios of line strengths for the stronger transitions are much closer to values expected from purely angular recoupling considerations. The $3p_{3/2}:3p_{1/2}$ ratio for Si^{3+} was 2.002. The $3p \rightarrow 4s$ transition ratio has a slight deviation from 2, with the MBPT-SD calculations giving 2.015 for Mg^+ and 2.006 for Si^{3+} (the BSR-CI ratios are similar).

The better than 0.5% agreement between the model potential and MBPT-SD line strengths for strong transitions is consistent with previous comparisons. The general level of agreement between calculations with a semiempirical core potential and more sophisticated *ab initio* approaches for properties such as oscillator strengths, polarizabilities, and dispersion coefficients has generally been very good [31,65–67]. There was a tendency for the agreement between the HFCP and MBPT-SD line strengths to degrade slightly from Mg^+ and Si^{3+}. This is probably due to the increased importance of relativistic effects as the nuclear charge increases.

C. Polarizabilities

The polarizabilities of the $3s$, $3p$, and $3d$ levels of Mg^+ and Si^{3+} as computed by the HFCP and MBPT-SD calculations are listed in Table IV. Tensor polarizabilities are also determined for the $3p$ and $3d$ levels. Definitions of the tensor polarizability, $\alpha_{1,2,J,J}$, in terms of oscillator strength sum rules can be found in Refs. [68,69].

Table V gives a short breakdown of the contributions of different terms to the dipole polarizability while Table VI gives the breakdown for the quadrupole polarizability. The $3s \rightarrow \varepsilon p(d)$ contribution represents anything over $n=6$ and can be regarded as a mix of some higher discrete states as well as the pseudocontinuum. Polarizabilities for the Mg^+ and Si^{3+} ground states from other sources are also listed in

TABLE III. Line strengths (in a.u.) for various transitions of Mg^+ and Si^{3+}. The line strengths are mainly for dipole transitions with the exception of the $3s \rightarrow 3d$ and $3s \rightarrow 4d$ transitions.

	Mg^+			Si^{3+}		
Transition	HFCP	MBPT-SD	BSR-CI	HFCP	MBPT-SD	BSR-CI
$S^{(1)}_{3s\text{-}4p_{1/2}}$	0.00251	0.00261	0.00211	0.0382	0.0385	0.0385
$S^{(1)}_{3s\text{-}4p_{3/2}}$	0.00501	0.00460	0.00362	0.0764	0.0744	0.0738
$S^{(1)}_{3s\text{-}5p_{1/2}}$	0.00395	0.00402	0.00366	0.0138	0.0139	0.0138
$S^{(1)}_{3s\text{-}5p_{3/2}}$	0.00790	0.00763	0.00692	0.0276	0.0270	0.0268
$S^{(1)}_{3p_{1/2}\text{-}4s}$	2.887	2.868	2.886	0.6410	0.6334	0.6328
$S^{(1)}_{3p_{3/2}\text{-}4s}$	5.773	5.779	5.815	1.282	1.284	1.283
$S^{(1)}_{3p_{1/2}\text{-}5s}$		0.2117	0.2115		0.0633	0.0629
$S^{(1)}_{3p_{3/2}\text{-}5s}$		0.4247	0.4243		0.1284	0.1267
$S^{(1)}_{3p_{1/2}\text{-}3d_{3/2}}$	17.32	17.29	17.35	5.923	5.933	5.955
$S^{(1)}_{3p_{3/2}\text{-}3d_{3/2}}$	3.463	3.468	3.482	1.185	1.190	1.195
$S^{(1)}_{3p_{3/2}\text{-}3d_{5/2}}$	31.17	31.21	31.33	10.66	10.71	10.75
$S^{(1)}_{3p_{1/2}\text{-}4d_{3/2}}$	0.4100	0.4168	0.4631	0.0234	0.0212	0.0204
$S^{(1)}_{3p_{3/2}\text{-}4d_{3/2}}$	0.0820	0.0825	0.0918	0.00468	0.00455	0.00438
$S^{(1)}_{3p_{3/2}\text{-}4d_{5/2}}$	0.7380	0.7423	0.8291	0.0421	0.0410	0.0395
$S^{(2)}_{3s\text{-}3d_{3/2}}$	97.52	97.51		16.81	16.85	
$S^{(2)}_{3s\text{-}3d_{5/2}}$	146.3	146.3		25.21	25.27	
$S^{(2)}_{3s\text{-}4d_{3/2}}$	3.615	3.638		0.2732	0.2659	
$S^{(2)}_{3s\text{-}4d_{5/2}}$	5.422	5.455		0.4098	0.3986	

Tables V and VI. The HFCP Mg^+ polarizability is marginally smaller than that reported previously [18] since the present evaluation includes a small core-valence correction.

The very good agreement between the HFCP and MBPT-SD polarizabilities is a notable feature of Table IV. None of the static polarizabilities differ by more than 0.5% with the exception being the α_2 of the Mg^+ $3d$ state. Here the difference is caused by the very small $\Delta E_{3d\text{-}4s}$ energy difference which is sensitive to small errors in the HFCP energies. The relative difference between some of the tensor polarizabilities is larger, but this is due to cancellations between the

TABLE IV. The polarizabilities for the $3s$, $3p$, and $3d$ states of Mg^+ and Si^{3+}. The tensor polarizabilities are for the $M_J=J$ states. For states with $\ell>0$, the MBPT-SD average values represent the weighted values for the spin-orbit doublet.

	α_1 (a.u.)		$\alpha_{1,2JJ}$ (a.u.)		α_2 (a.u.)		α_3 (a.u.)	
State	HFCP	MBPT-SD	HFCP	MBPT	HFCP	MBPT-SD	HFCP	MBPT-SD
$Mg^+(3s)$	34.99	35.05	0	0	156.1	156.1	1715	1719
$Mg^+(3p_{1/2})$		31.60	0	0		340.2		11778
$Mg^+(3p_{3/2})$		31.88	1.162	1.156		343.0		11879
$Mg^+(3p$-average)	31.79	31.79			341.7	342.1	11839	11845
$Mg^+(3d_{3/2})$		189.3	−78.47	−79.15		−9336		2.857×10^5
$Mg^+(3d_{3/2})$		188.6	−112.1	−112.2		−9341		2.860×10^5
$Mg^+(3d$-average)	189.5	188.9			−9611	−9339	2.855×10^5	2.859×10^5
$Si^{3+}(3s)$	7.399	7.419	0	0	12.13	12.15	47.03	47.15
$Si^{3+}(3p_{1/2})$		3.120	0	0		13.05		155.1
$Si^{3+}(3p_{3/2})$		3.183	1.459	1.462		13.21		157.1
$Si^{3+}(3p$-average)	3.158	3.162			13.17	13.16	156.3	156.5
$Si^{3+}(3d_{3/2})$		5.168	−0.6083	−0.631		58.61		695.2
$Si^{3+}(3d_{5/2})$		5.131	−0.8690	−0.848		58.61		696.2
$Si^{3+}(3d$-average)	5.135	5.146			58.43	58.61	693.2	695.8

TABLE V. Breakdown of the different contributions to the dipole polarizabilities of Mg^+ and Si^{3+}. The ϵp contribution includes both pseudostate and continuum states. Dipole polarizabilities from other sources are also listed with citation. The estimated uncertainties for the different components of the uncertainty are given in brackets. The RESIS reanalysis are taken from the reanalysis of the RESIS fine-structure intervals described later.

	Mg^+		Si^{3+}	
Quantity	HFCP	MBPT-SD	HFCP	MBPT-SD
$3s \rightarrow 3p$	34.413	34.478(100)	7.153	7.180(6)
$3s \rightarrow (4-6)p$	0.021	0.020(0)	0.054	0.053(0)
$3s \rightarrow \epsilon p$	0.091	0.087(4)	0.030	0.029(1)
Core	0.481	0.481(10)	0.162	0.162(8)
Core-valence	−0.018	−0.018(2)	−0.005	−0.005(1)
Total	34.99	35.05(12)	7.394	7.419(16)
CI [29]	35.66		7.50	
RESIS [5,6]	35.00(5)		7.426(12)	
Laser Expt. [56]	33.80(50)			
f sums [57]	35.1			
RCC [30]	35.04			
RESIS reanalysis	35.04(3)		7.433(25)	

component sum rules that are combined to give the tensor polarizability.

A recent CI calculation of the Mg^+ and Si^{3+} ground state dipole polarizabilities [29] gave polarizabilities that were 1–2 % larger than the HFCP and MBPT-SD polarizabilities. The more recent RCC [30] gave polarizabilities that were compatible with the present values.

The dipole polarizabilities for both Mg^+ and Si^{3+} are dominated by the resonant oscillator strength. For Mg^+ one finds that 98.3% of α_1 arises from the $3s \rightarrow 3p$ transition. For Si^{3+} the contribution is smaller but still substantial at 96.7%. The nonadiabatic dipole polarizabilities are even more dominated by the contribution from the resonant transition. One finds that 99.9% of β_1 and 99.99% of γ_1 for Mg^+ come from this transition. The proportions for the Si^{3+} β_1 and γ_1 are 99.6% and 99.92%, respectively.

TABLE VI. Breakdown of the different contributions to the quadrupole polarizabilities of Mg^+ and Si^{3+}. The ϵp contribution includes both pseudostate and continuum states. The quadrupole polarizabilities from a RESIS analysis is listed.

	Mg^+		Si^{3+}	
Quantity	HFCP	MBPT-SD	HFCP	MBPT-SD
$3s \rightarrow 3d$	149.69	149.68(32)	11.502	11.529(9)
$3s \rightarrow (4-6)d$	4.99	5.01(4)	0.240	0.235(0)
$3s \rightarrow \epsilon d$	0.86	0.85(6)	0.289	0.280(8)
Core	0.52	0.52(6)	0.102	0.102(12)
Total	156.1	156.1(5)	12.13	12.15(3)
RESIS [5,6]	222(54)			
RCC [30]	156.0			

TABLE VII. The polarizabilities and C_n parameters computed from the composite list of HFCP and MBPT-SD matrix elements. The parameters tabulated here can be regarded as the recommended theoretical values. The C_7, C_8, and C_{8L} parameters were used in the analysis the RESIS spectra for Mg^+ and Si^{3+}. The B_4 and B_6 values are derived from the polarization plot analysis of the RESIS energy intervals. The B_6 uncertainties are purely statistical in nature while the B_4 uncertainties take into account systematic errors resulting from the use of Eq. (1).

Quantity	Mg^+	Si^{3+}
α_1	35.05(12)	7.419(16)
α_2	156.1(5)	12.15(3)
α_3	1715(6)	47.03(12)
β_1	106.0(3)	11.04(1)
β_2	236.1(5)	8.065(6)
γ_1	324.7(9)	16.82(1)
α_{112}	2416(52)	89.74(41)
α_{1111}	3511(90)	51.19(28)
C_4	17.53(6)	3.710(8)
C_6	−240.1(12)	−27.06(4)
C_7	−1727(27)	−125.6(2)
C_8	10672(92)	553.1(6)
C_{8L}	1169(3)	60.54(5)
B_4	17.522(15)	3.716(12)
B_6	−251.2(79)	−30.96(134)

The quadrupole polarizabilities are also dominated by a single transition. Table VI shows that the $3s \rightarrow 3d$ excitation constitutes at least 95% of α_2 for both Mg^+ and Si^{3+}.

Table VII lists gives the polarizabilities from a composite list of matrix elements. These polarizabilities combine the best features of the HFCP and MBPT-SD calculations and can be regarded as the recommended set of polarizabilities.

The HFCP calculation automatically generated a file containing matrix elements between every state included in the basis. The more computationally intensive MBPT-SD calculation were used to replace the largest and most important matrix elements in the HFCP lists. The HFCP matrix elements for the $3s \rightarrow 3p$, $3p \rightarrow 3d$, $3s \rightarrow 3d$, and $3p \rightarrow 4s$ transitions were replaced by J weighted averages of the equivalent MBPT-SD matrix elements. The HFCP matrix elements were retained for the $3s \rightarrow \varepsilon p(d)$ remainders since they are more accurate than the RPA-DF matrix elements that were part of the MBPT-SD evaluation. It did not matter whether HFCP or MBPT-SD matrix elements were retained for the $3s \rightarrow (4-6)p(d)$ excitations since these matrix elements were very small and there was not much difference between the HFCP and MBPT-SD matrix elements. This use of a composite list of matrix elements combined the higher accuracy of the MBPT-SD calculation for the most important low-lying transitions with the computational convenience of the marginally less accurate HFCP calculation.

The only difference between Table VII and MBPT-SD polarizabilities occurs for α_3. A relatively large part of α_3

comes from the higher excited states and the continuum. Accumulating a lot of small contributions is tedious for the computationally expensive MBPT-SD, so this is done with the less accurate DF approach. In this case the HFCP polarizability was probably more accurate than the MBPT-SD polarizability. It should be noted that the octupole polarizability is of minor importance in the subsequent analysis.

The composite list of matrix elements was also used for the calculation of the third-order α_{112} polarizability and the fourth-order α_{1111} polarizability. The biggest change in α_{112} and α_{1111} resulting from using the composite matrix element list was less than 0.3%. The α_{112} and α_{1111} polarizabilities did not allow for contributions from the core. The impact of the core will be small due to large energy difference involving core excitations. The relative effect of the core for α_{112} and α_{1111} can be expected to be about as large as the core effect in the ground state α_1 and α_2 since there are core excitations that contribute with only one core energy in the energy denominator. For example, consider the α_{112} excitation sequence of $2p^6 3s\ ^2\mathrm{S}^e \rightarrow 2p^5 3s 3d\ ^2\mathrm{P}^o \rightarrow 2p^6 3d\ ^2\mathrm{D}^e \rightarrow 2p^6 3s\ ^2\mathrm{S}^e$.

The numerical procedures used to generate the α_{112} and α_{1111} polarizabilities were validated for He^+. A calculation of the He^+ excitation spectrum was performed and the resulting lists of reduced matrix elements were entered into the polarizability programs. All the coefficients given by Drachman [70] were reproduced.

D. Error assessment

Making an *a priori* assessment of the accuracy of the HFCP polarizabilities is problematic since they are semiempirical in nature. The error assessment for the MBPT-SD proceeds by assuming that the total contribution of fourth- and higher-order terms omitted by the SD all-order method does not exceed the contribution of already included fourth- and higher-order terms. Thus, the uncertainty of the SD matrix elements is estimated to be the difference between the SD all-order calculations and third-order results.

This procedure was applied to the $S_{3s\text{-}3p_{1/2}}$ line strength of sodium yielding an uncertainty $\delta S_{3s\text{-}3p_{1/2}}=0.092$. This uncertainty exceeds the difference between the SD line strength of 12.47 [26] and recent high precision experiments which give 12.412(16) [45,46], and 12.435(41) [47]. A similar situation applies for the $S_{3s\text{-}3p_{3/2}}$ line strength.

A detailed first principles evaluation of the uncertainty of the Si^{3+} static dipole polarizability has been done and the uncertainty budget is itemized in Table V. In this case, the difference between the SD line strength and third-order line strength for the resonance transition was 0.082%. The uncertainties in the remaining $(n=4-6)$ discrete transitions were of similar size. Uncertainties in the energies used in the oscillator strength sum rule can be regarded as insignificant since experimental energies were used. To estimate the accuracy of the remainder of the valence sum, the $(n=4-6)$ calculation was repeated using RPA matrix elements and DF energies. The difference of 3% between the MBPT-SD and DF-RPA values was assessed to be the uncertainty in the εp remainder. The good agreement between the HFCP and DF-RPA values for the nonresonant valence contribution gives additional evidence that the uncertainty estimate is realistic.

The core dipole polarizability calculated in the RPA is known to underestimate the actual core polarizability. For neon, the RPA gives $\alpha_1=2.38$ a.u. [36] which is 11% smaller than the experimental value of 2.669 a.u. [71]. For Na^+, the RPA gives 0.9457 a.u. [36] while experiment gives 1.0015(15) a.u. [72]. The pseudonatural orbital approach used for Mg^{2+} gave $\alpha_1=2.67$ a.u. for Ne [73] and $\alpha_1=0.9947$ a.u. for Na^+ [23]. The uncertainty in the quadrupole core polarizability is based on comparisons with coupled cluster calculations for neon [74,75]. The RPA value of 6.423 a.u. is about 12% smaller than the coupled cluster values of 7.525 a.u. [75] and 7.525 a.u. [74]. The relative uncertainties are $\delta\alpha_1(Mg^{2+})=2\%$, $\delta\alpha_1(Si^{4+})=5\%$, $\delta\alpha_2(Mg^{2+})=12\%$, and $\delta\alpha_2(Si^{4+})=12\%$. The core-valence correction was assigned an uncertainty of 20% based on differences between DF and RPA matrix elements. The RPA error estimates are likely to be very conservative since the uncertainty in the RPA polarizabilities is expected to decrease as the nuclear charge increases.

Combining the uncertainties in the valence and core polarizabilities for Si^{3+} gives a final uncertainty of 0.16 a.u. (or 0.22%) in the MBPT-SD α_1.

The uncertainty in the Si^{3+} α_2 listed in Table VI was evaluated with a process that was similar to the dipole polarizability. The difference between the SD line strength and third order line strength for the $3s \rightarrow 3d_{5/2}$ transition was 0.064% (the relative uncertainty was almost the same for the transition to the $3d_{3/2}$ state). This uncertainty is slightly smaller than that for the resonant dipole transition. This was expected since the $3d$ electron is further away from the nucleus than the $3p$ electron and therefore correlation-polarization corrections have less importance. Rather than do a computationally expensive analysis, the relative uncertainties in the $(nd+\epsilon d)$ remainders were conservatively assigned to be same as those for the dipole transitions. The final uncertainty was $\delta\alpha_2=0.03$ a.u..

The relative uncertainties in the Mg^+ polarizabilities are set in the same way as Si^{3+}. The difference between the third-order and all-order dipole line strengths for the resonance transition was 0.3%. The relative differences were larger for the $n=4-6$ transitions due to their small size. For example, the third-order to all-order comparison for the $S_{3s\text{-}4p}$ multiplet strength gave 5%. This is consistent with the difference with the experimental multiplet strength. The uncertainties were slightly smaller for the slightly larger $5p$ and $6p$ transitions. However, the net contribution to the uncertainty was miniscule since the line strengths were so small. The $3s \rightarrow \varepsilon p$ uncertainty of 5% was based on differences between the HFCP and DF-RPA matrix elements.

The $n=3-6$ transition uncertainties in the Mg^+ α_2 polarizability listed in Table VI were derived from the third-order to all-order comparison. The relative uncertainty in the $3s \rightarrow 3d$ transition was 0.22%. The very good agreement between the HFCP and MBPT-SD values for these terms is further supportive of a small uncertainty for the $n=3-6$ transitions. The 7% uncertainty in the $3d \rightarrow \varepsilon d$ remainder was based on the differences between the MBPT-SD and DF matrix elements.

TABLE VIII. Various energy corrections (in units of MHz) for the $n=17$ intervals of Mg^+ and the $n=29$ intervals of Si^{3+}. These were computed using C_n values of Table VII.

n	L_1	L_2	ΔE_{rel}	ΔE_4	ΔE_6	ΔE_7	ΔE_8	ΔE_{8L}	ΔE_{sec}	ΔE_{ss}
					Mg^+					
17	6	7	0.7314	1555.7935	−53.7751	−20.4880	7.1989	31.5551	8.1506	−0.1122
17	7	8	0.5593	678.8962	−12.6733	−3.4612	0.8512	4.9308	1.5012	−0.1702
17	8	9	0.4416	326.8907	−3.5557	−0.7292	0.1327	0.9816	0.3393	−0.2320
17	9	10	0.3575	169.8765	−1.1373	−0.1808	0.0253	0.2325	0.0896	−0.2723
17	10	11	0.2953	93.8138	−0.4026	−0.0508	0.0056	0.0627	0.0267	−0.3039
					Si^{3+}					
29	8	9	7.2052	1172.2322	−67.1286	−27.9320	11.3800	83.6138	2.4220	−0.1658
29	9	10	5.8328	614.9317	−22.2670	−7.2876	2.3124	21.0913	0.6574	−0.3049
29	10	11	4.8184	343.2123	−8.2257	−2.1728	0.5526	6.1258	0.2026	−0.4199
29	11	12	4.0474	201.5328	−3.3152	−0.7211	0.1502	1.9896	0.0693	−0.6026
29	11	13	7.4953	324.9889	−4.7508	−0.9824	0.1956	2.6972	0.0951	−1.3540
29	11	14	10.4675	403.3750	−5.4110	−1.0843	0.2106	2.9685	0.1054	−2.3123

The relative uncertainties in the octupole polarizabilities listed in Table VII were set to the uncertainties in the quadrupole polarizabilities. The nf orbitals are further away from the core than the $3d$ orbitals and so the α_2 uncertainty serves as a convenient overestimate.

The uncertainties in the higher-order polarizabilities β_1, β_2, and γ_1 listed in Table VII were taken to be the uncertainties in the resonant line strengths. The higher powers in the energy denominator means other transition make a negligible contribution.

The uncertainties in α_{112} and α_{1111} were derived from the uncertainties in the reduced matrix elements. The relative uncertainties for the most important $3s \rightarrow 3p$, $3p \rightarrow 3d$, and $3s \rightarrow 3d$ matrix elements were simply added to give relative uncertainties for valence part of α_{112} and α_{1111}. The relative uncertainty resulting from the omission of core excitations was taken as the ratio of the core to total dipole polarizability. This was added to the α_{112} and α_{1111} uncertainties.

The uncertainties in C_6, C_7, C_8, and C_{8L} were determined by combining the uncertainties of the constituent polarizabilities. The most important of these parameters is the expected slope of the polarization plot, i.e., $\delta C_6 = \delta\alpha_2/2 + 3\delta\beta_1$. For Si^{3+} we obtain $\delta C_6 = 0.015 + 0.027 = 0.042$. For Mg^+ the uncertainty was $\delta C_6 = 1.2$.

V. POLARIZATION ANALYSIS OF RYDBERG STATES

A. The polarization interaction

The various polarizabilities needed for the polarization analysis were taken from composite calculation listed in Table VII. In this section we use the C_7, C_8, and C_{8L} values from Table VII to revisit the analysis of the RESIS data [5,6] and deduce improved values of the dipole and quadrupole polarizabilities.

Estimates of C_7 and C_{8L} were previously made by Snow and Lundeen [5] using MBPT-SD transition amplitudes for the lowest lying transitions. These earlier estimates are within a few percent of the present more sophisticated analysis. The Snow and Lundeen values for C_7 were −1684(9) a.u. for Mg^+ and −122(9) a.u. for Si^{3+}. They are a few percent smaller than those listed in Table VII due to the omission of higher excitations from the sum rule. The Snow and Lundeen values for C_{8L} were 1170(12) a.u. for Mg^+ and 60.5 a.u. for Si^{3+}.

One aspect of Table VII that is relevant to the interpretation of experiments is the importance of the nonadiabatic dipole polarizabilities. Consider Mg^+, for example. The respective contributions to C_6 are 78.05 a.u. from α_2 and −318.0 a.u. from $-6\beta_2$. Similarly, one finds that the γ_1 term of -1.6×324.7 makes up 30% of the final C_7 value of −1727 a.u. And finally, one finds that the C_8 value of 10 672 is largely due to the $36\gamma_1$ contribution of 11 689 a.u. The degree of importance of the nonadiabatic terms scarcely diminishes for the Si^{3+} ion.

Table VIII gives the energy shifts to the $n=17$ levels of Mg^+ and the $n=29$ levels of Si^{3+} using the values in Table VII. The energy shifts need $\langle r^{-n} \rangle$ expectation values which were evaluated using the formulas of Bockasten [76].

B. The polarization plot

Polarizabilities can be extracted from experimental data by using a polarization plot. This is based on a similar procedure that is used to determine the ionization limits of atoms [77]. The notations B_4 and B_6 (instead of C_4 and C_6) are used to denote the polarization parameters extracted from the polarization plot analysis. This is to clearly distinguish them from polarization parameters coming from atomic structure calculation. Assuming the dominant terms leading to departures from hydrogenic energies are the B_4 and B_6 terms, one can write

$$\frac{\Delta E}{\Delta\langle r^{-4}\rangle} = B_4 + B_6 \frac{\Delta\langle r^{-6}\rangle}{\Delta\langle r^{-4}\rangle}. \tag{23}$$

In this expression, ΔE is the energy difference between two states of the same n but different L, while $\Delta\langle r^{-6}\rangle$ and $\Delta\langle r^{-4}\rangle$

are simply the differences in the radial expectations of the two states.

There are other corrections that can result in Eq. (23) departing from a purely linear form [5,6]. These are relativistic energy shifts, Stark shifts due to a residual electric field, and polarization shifts due to the C_7, C_8 (and possibly higher-order) terms of Eq. (1). The energy difference between the (n,L) and (n,L') states can be written

$$\Delta E = \Delta E_4 + \Delta E_6 + \Delta E_7 + \Delta E_8 + \Delta E_{8L} + \Delta E_{\rm rel} + \Delta E_{\rm sec} + \Delta E_{\rm ss}, \tag{24}$$

where ΔE_n arises from the polarization terms of order $\langle r^{-n}\rangle$.

Dividing through by $\Delta\langle r^{-4}\rangle$ and replacing ΔE_6 by $B_6\Delta\langle r^{-6}\rangle$ gives

$$\frac{\Delta E}{\Delta\langle r^{-4}\rangle} = B_4 + B_6\frac{\Delta\langle r^{-6}\rangle}{\Delta\langle r^{-4}\rangle} + \frac{\Delta E_7 + \Delta E_8 + \Delta E_{8L}}{\Delta\langle r^{-4}\rangle} + \frac{\Delta E_{\rm rel} + \Delta E_{\rm sec} + \Delta E_{\rm ss}}{\Delta\langle r^{-4}\rangle}. \tag{25}$$

The influence of the Stark shifts, relativistic shifts, and second-order polarization correction can be incorporated into the polarization plot by simply subtracting the energy shifts. The corrected energy shift, $\Delta E_{\rm c1}$, is defined as

$$\frac{\Delta E_{c1}}{\Delta\langle r^{-4}\rangle} = \frac{\Delta E_{\rm obs}}{\Delta\langle r^{-4}\rangle} - \frac{\Delta E_{\rm rel} + \Delta E_{\rm sec} + \Delta E_{ss}}{\Delta\langle r^{-4}\rangle}. \tag{26}$$

An approximate expression is used for the relativistic energy correction. This is taken from the result

$$E_{\rm rel} = -\frac{\alpha^2 Z^4}{2n^3}\left(\frac{1}{j+1/2} - \frac{3}{4n}\right). \tag{27}$$

The correction due to second-order effects, $\Delta E_{\rm sec}$, uses the expressions of Drake and Swainson [78–80]. The calculation of the second-order energy shift requires an estimate of the dipole polarizability. This was taken from Table VII.

The Stark shift corrections use the Stark shift rates from Snow and Lundeen [5,6] and the deduced electric field. The energy corrections due to relativistic and polarization effects for the states of Mg^+ and the Si^{3+} for which RESIS data existed are listed in Table VIII.

The second corrected energy is defined by further subtracting the polarization shifts, ΔE_7, ΔE_8, and ΔE_{8L},

$$\frac{\Delta E_{c2}}{\Delta\langle r^{-4}\rangle} = \frac{\Delta E_{\rm c1}}{\Delta\langle r^{-4}\rangle} - \frac{\Delta E_7 + \Delta E_8 + \Delta E_{8L}}{\Delta\langle r^{-4}\rangle}. \tag{28}$$

Finite mass effects were taken into consideration when the various energy shifts were computed. However, these effects have a relatively small influence on the analysis. The first-order finite mass effect is largely eradicated due to cancellations between adjacent (n,L) levels. The finite mass effect in the various correction terms is quite small.

C. Mg^+

Tables VIII shows that the energy splitting between adjacent L Rydberg levels is dominated by the C_4 term. The next biggest term is the ΔE_6 term which is 3% of ΔE_4 for the (17,6)-(17,7) interval. The ΔE_{8L} correction is larger than ΔE_7. The relative impact of the higher-order corrections diminishes as L increases. However, the relative importance of the Stark shift, $\Delta E_{\rm ss}$, starts to increase as L increases.

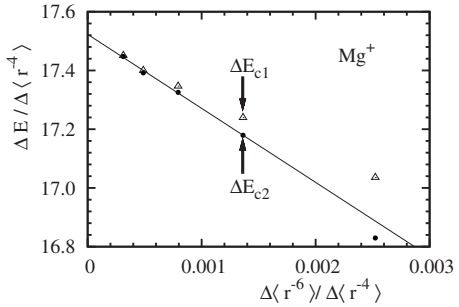

FIG. 1. The polarization plot of the fine-structure intervals of Mg for the $n=17$ Rydberg levels. The ΔE_{c1} intervals are corrected for relativistic, second-order, and Stark shifts. The ΔE_{c2} intervals account for $\langle r^{-7}\rangle$ and $\langle r^{-8}\rangle$ shifts. The linear regression for the $\Delta E_{\rm c2}$ plot did not include the last point.

The revised analysis of the RESIS energy intervals for Mg^+ was performed by subtracting the $\Delta E_{\rm c1}$ and $\Delta E_{\rm c2}$ energy corrections itemized in Table VIII from the observed energy splittings. This represents a refinement over the previous analysis by Snow and Lundeen [6] in a couple of respects. First, Snow and Lundeen did not include the C_8 term since the necessary polarizability information simply was not available. Their evaluation of α_{112} only included the $3p$ and $3d$ states in the intermediate sums. The truncation of the sums in the α_{112} calculation was justified as the correction to α_{112} from a more complete evaluation was only a few percent. The impact of the ΔE_8 shift is more substantial. Table VIII shows the relative size of ΔE_8 with respect to ΔE_7 ranging from 35% to 11%.

Figure 1 shows the polarization plot for Mg^+. One set of data points plots $\Delta E_{\rm c1}/\Delta\langle r^{-4}\rangle$ against $\Delta\langle r^{-6}\rangle/\Delta\langle r^{-4}\rangle$. The other set of data points shows $\Delta E_{\rm c2}/\Delta\langle r^{-4}\rangle$ against $\Delta\langle r^{-6}\rangle/\Delta\langle r^{-4}\rangle$. Linear regression was applied to the four data points with $\Delta\langle r^{-6}\rangle/\Delta\langle r^{-4}\rangle < 0.002$. The (17,6)-(17,7) interval was omitted from the fit because the influence of $\Delta E_{7,8,8L}$ and $\Delta E_{\rm sec}$ amount to just over 50% of ΔE_6. Visual examination of Fig. 1 shows this data point lies a significant distance away from the line of best fit obtained from the four remaining points. The linear regression gave an intercept of $B_4 = 17.522(7)$ a.u. and a slope of $B_6 = -251.2(79)$ a.u. The quoted uncertainties are the statistical uncertainties from the linear regression fit. The present B_6 is about 25% larger than the B_6 of −198(23) from the original Snow and Lundeen analysis.

The new value of the dipole polarizability derived from the polarization plot intercept was 35.044 a.u. This is marginally larger than the polarizability of 35.00(5) a.u. given in the original Snow and Lundeen analysis [6]. The present α_1 is larger because the additional corrections in the $\Delta E_{\rm c2}$ energies lead to a steeper polarization plot.

The slope of $B_6 = -251.2(79)$ is slightly steeper than the Table VII recommended C_6 of −240.1(12). Using the slope of −251.2 in conjunction with a $\beta_1 = 106.0$ a.u. gives a quad-

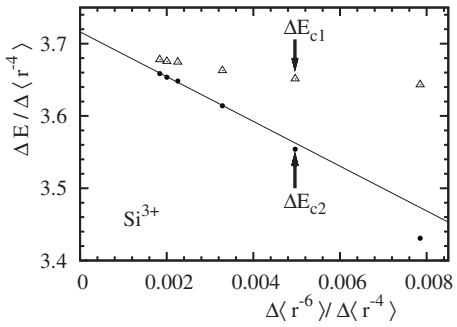

FIG. 2. The polarization plot of the fine-structure intervals of Si^{2+} for the $n=29$ Rydberg levels. The ΔE_{c1} intervals are corrected for relativistic, second-order, and Stark shifts. The ΔE_{c2} intervals account for $\langle r^{-7}\rangle$ and $\langle r^{-8}\rangle$ shifts. The linear regression for the ΔE_{c2} plot did not include the last two points.

rupole polarizability of $\alpha_2=-502.4+636.3=133.9$ a.u. This is about 90 a.u. smaller than the polarizability of 222(54) a.u. given by Snow and Lundeen [6]. However it is only 22 a.u. smaller than the theoretical polarizabilities of 156.1 a.u. The uncertainty in the derived quadrupole polarizability would be $(2\times7.9+6\times0.3)=17.6$. The RESIS and theoretical values are slightly outside their respective combined error estimates. However, the uncertainty estimate used for C_6 is purely statistical in nature and does not allow for higher-order corrections to Eq. (23). This point is discussed in more detail later.

The relatively large change in α_2 from 222(54) to 134(18) a.u. was caused by the inclusion of ΔE_8. There is a near cancellation between some of the ΔE_7 and ΔE_{8L} energy corrections. Hence the inclusion of the ΔE_8 energy correction had a relatively large impact. For example, the sum of ΔE_7 and ΔE_{8L} for the (17,7)-(17,8) interval was 1.473 MHz. The ΔE_8 correction was 0.851 MHz.

The derived dipole polarizability and value of B_6 are not sensitive to small changes in the C_n values used for the corrections. An analysis using alternate C_n values derived from the uncertainties detailed in Table VII was performed. This resulted in an additional uncertainty of 0.0004 a.u. in B_4 and an additional uncertainty of 1.6 in B_6. These additional uncertainties were sufficiently small to ignore in subsequent analysis.

D. Si^{3+}

The polarization plot for Si^{3+} is shown in Fig. 2. The most notable feature is the large difference between the ΔE_{c1} and ΔE_{c2} data sets. The other noteworthy feature is the pronounced deviation from linear of the $\frac{\Delta E_{c2}}{\Delta\langle r^{-4}\rangle}$ plot.

Examination of Table VIII for the (29,8)-(29,9) interval shows that the net $\Delta E_{7,8,8L}$ correction is very close in magnitude to the ΔE_6 energy correction. The $\Delta E_{7,8,8L}$ correction is still more than 50% of the ΔE_6 correction for the (29,10)-(29,11) interval. The polarization series is an asymptotic series [70,81] and is not absolutely convergent as n increases. As mentioned by Drachman [70], a condition for the usefulness of the polarization series is that the $\Delta E_{7,8,8L}$ corrections should be significantly smaller than the ΔE_6 corrections. This condition is not satisfied for the first two intervals and leads to the noticeable curvature in the plot of the ΔE_{c2} data points.

The resolution to this problem would be to increase the L values at which the intervals are measured. But Stark shift corrections become increasingly important at high L. The Stark shift corrections are significant for the (29,11)-(29,14) interval.

A line of best fit was drawn using the four data points with $\Delta\langle r^{-6}\rangle/\Delta\langle r^{-4}\rangle<0.004$. The linear regression gave an intercept of $B_4=3.7163(32)$ and a slope of $B_6=-30.96(134)$. The intercept translates to a polarizability of 7.433 a.u. To put this in perspective, the polarizability originally deduced from the RESIS experiment was 7.408(11) [4]. A later analysis which included the C_7 and C_{8L} potentials gave 7.426(12) a.u. [5]. There has been a steady increase in the derived dipole polarizability as more higher-order terms in the polarization series are incorporated into the analysis.

The polarization plot B_6 of −30.96(134) was about 10% larger in magnitude than the MBPT-SD value of −27.06(5). This value of B_6 results in a quadrupole polarizability of $\alpha_2=(-2\times30.96+6\times11.04)=4.34$ a.u. which is 60% smaller than the HFCP and MBPT-SD polarizabilities. The uncertainty of $(2\times1.34+6\times0.006)=3.0$ a.u. is too small to allow consistency with the theoretical values.

E. An alternate perspective on the polarization plot analysis

The analysis so far can be regarded as a standard polarization analysis but with additional refinements due to improved knowledge about the higher-order terms in the polarization series. However, it is worth recalling that Eq. (1) is an asymptotic expansion [70,81] so there is always some uncertainty about when the expansion should be terminated. This raises the specter that the derived B_4 and B_6 coefficients are influenced by systematic errors arising from the termination point of the series, Eq. (1). This is quite likely since the higher-order polarization corrections (not to mention Stark shifts) range from to 30–100 % of the raw C_6 energy shifts.

In this section we take the attitude that the experimental B_6 coefficient will be polluted by systematic errors relating to the use of Eq. (1). So the main differences between the atomic structure C_6 values and the polarization plot B_6 values are asserted to be inherent to the use of Eq. (1) rather than imperfections in the atomic structure calculations. The comparison between the present atomic structure theories and the RESIS experiment has resulted in agreement to better than 0.5% for dipole polarizabilities in conformity with the first principles error analysis of the atomic structure dipole polarizabilities. Under such circumstances it is not credible to postulate large errors in the atomic structure C_6 on the basis of the polarization analysis of the RESIS energy intervals.

Systematic errors arising from Eq. (1) can potentially affect the derived value of B_4 since an incorrect value for the polarization plot slope will change its intercept. The inclusion of this additional source of systematic error was taken into consideration for Mg^+ as follows. The linear regression analyses of the polarization plot were redone with a series of

fixed B_6 values that were constrained to lie within -251.2 ± 19.0. The uncertainty of 19.0 in the allowable range for B_6 was derived by adding the statistical uncertainty of 7.9 from the initial linear regression fit to $|240.1–251.2|$, i.e., the difference between B_6 and the atomic structure C_6 of Table VII. This gave a revised uncertainty of $\delta B_4 = 0.015$, leading to a final α_1 of 35.04(3) a.u. The same analysis was repeated for Si^{3+}. In this instance the derived value of α_1 was 7.433(25) a.u.

The large uncertainties in B_6 do not detract greatly from the precision of the dipole polarizability. One of the reasons higher-order effects can have a large impact on B_6 is that ΔE_6 is small because of the cancellations between α_2 and β_1. However, the small size of B_6 means a large uncertainty in B_6 has a relatively small impact on the derived α_1.

F. Estimate of the resonant oscillator strengths

As the polarizabilities are dominated by the resonant transition it is possible to derive an estimate for the resonant multiplet strength [82]. We use the relation

$$S_{3s-3p} = \frac{\alpha_1 - \alpha_1' - \alpha_{\rm core}}{\frac{2}{9\Delta E_{3s-3p_{1/2}}} + \frac{4}{9\Delta E_{3s-3p_{3/2}}}}. \tag{29}$$

In this expression α_1 is the polarizability extracted from the polarization plot while $\alpha_{\rm core}$ is the net core polarizability, and α_1' is the valence polarizability excluding the resonant transition. For the Mg^+ multiplet, we use

$$S_{3s-3p} = \frac{35.044 - 0.112 - 0.463}{4.08436} = 8.439. \tag{30}$$

Using the uncertainties detailed earlier, 0.03 for α_1, 0.004 for α_1', and 0.010 for $\alpha_{\rm core}$, the final value is 8.439(11). This is equivalent to a line strength of $S_{3s\text{-}3p_{3/2}} = 11.25(2)$, in agreement with the recent experimental value of 11.24(6) [51].

Repeating the analysis for Si^{3+} gave a multiplet strength of 3.519(16) for the $3s \rightarrow 3p$ transition. This is equivalent to $S_{3s-3p_{3/2}} = 4.693(24)$ which is 0.14% larger than the MBPT-SD line strength of 4.686.

VI. CONCLUSIONS

A survey of polarization parameters of the Mg^+ and Si^{3+} ion states relevant to the analysis of the RESIS experiments by the Lundeen group [4–6] have been presented by two complementary approaches. The reanalysis of the fine-structure intervals gave dipole polarizabilities of 35.04(3) a.u. for Mg^+ and 7.433(25) a.u. for Si^{3+}. The HFCP and MBPT-SD calculations give polarizabilities that lie within 0.2% of each other for Mg^+ and 0.3% for Si^{3+}. The *ab initio* MBPT-SD dipole polarizabilities of 35.05(12) and 7.419(16) a.u., respectively, agree with the experimental dipole polarizabilities to accuracy of better than 0.3%.

One notable feature of the present analysis is the very good agreement between the HFCP and MBPT-SD calculations. Indeed, the MBPT-SD calculation agrees better with the computationally simple HFCP calculation than it does with two very large CI-type calculations. For example, the polarizabilities of the completely *ab initio* CI calculation [29] are about 1.5% larger than the MBPT-SD and HFCP polarizabilities. We conclude that a semiempirical calculation based on a HF core can easily be superior to a pure CI calculation unless the CI calculation is of very large dimension. The HFCP approach has the advantage of tuning the model energy levels to experiment and this goes a long way to ensuring that many of the interesting observables will be predicted accurately. There is one feature common to the HFCP and MBPT-SD approaches. Both approaches approximate the physics of the dynamical corrections beyond HF and DF methods, but within those approximations an effectively exact calculation is made.

There are two major sources of systematic error that can impact the interpretation of the RESIS experiment and have a major effect on the derived quadrupole polarizability. To a certain extent one has to choose the (n,L) states to navigate between excessively large nonadiabatic corrections and excessively large Stark shifts. If L is too small, then the $\Delta E_{7,8,8L}$ shift becomes larger than ΔE_6, thus invalidating the use of Eq. (1). On the other hand, Stark shift corrections become increasingly bigger as L becomes larger. These problems are most severe in Si^{3+} and are responsible for the slope of the polarization curve being different from the atomic structure predictions. An explicit two-state model of long-range polarization interactions is probably needed to realize the full potential of the RESIS experiment

ACKNOWLEDGMENT

This work was supported in part by the National Science Foundation Grant No. PHY-0758088.

[1] S. R. Lundeen, Adv. At., Mol., Opt. Phys. **52**, 161 (2005).
[2] R. J. Drachman, Phys. Rev. A **26**, 1228 (1982).
[3] R. J. Drachman and A. K. Bhatia, Phys. Rev. A **51**, 2926 (1995).
[4] R. A. Komara, M. A. Gearba, S. R. Lundeen, and C. W. Fehrenbach, Phys. Rev. A **67**, 062502 (2003).
[5] E. L. Snow and S. R. Lundeen, Phys. Rev. A **75**, 062512 (2007).
[6] E. L. Snow and S. R. Lundeen, Phys. Rev. A **77**, 052501 (2008).
[7] P. Gill, Metrologia **42**, S125 (2005).
[8] X. Baillard *et al.*, Eur. Phys. J. D **48**, 11 (2008).
[9] G. K. Campbell *et al.*, e-print arXiv:0804.4509.
[10] S. A. Diddams *et al.*, Science **293**, 825 (2001).
[11] A. Bauch, Meas. Sci. Technol. **14**, 1159 (2003).
[12] V. G. Pal'chikov, Y. S. Domnin, and A. V. Novoselev, J. Opt.

B: Quantum Semiclassical Opt. **5**, S131 (2003).
[13] S. G. Porsev and A. Derevianko, Phys. Rev. A **74**, 020502(R) (2006).
[14] T. Zelevinsky, M. M. Boyd, A. D. Ludlow, S. M. Foreman, S. Blatt, T. Ido, and J. Ye, Hyperfine Interact. **174**, 55 (2007).
[15] T. Rosenband *et al.*, Science **319**, 1808 (2008).
[16] W. M. Itano *et al.*, Proc. SPIE **6673**, 667303 (2007).
[17] B. Arora, M. S. Safronova, and C. W. Clark, Phys. Rev. A **76**, 064501 (2007).
[18] J. Mitroy and J. Y. Zhang, Eur. Phys. J. D **46**, 415 (2008).
[19] E. J. Angstmann, V. A. Dzuba, and V. V. Flambaum, Phys. Rev. Lett. **97**, 040802 (2006).
[20] E. L. Snow and S. R. Lundeen, Phys. Rev. A **76**, 052505 (2007).
[21] F. W. King, J. Mol. Struct. **400**, 7 (1997).
[22] W. D. Robb, M. R. Meadows, T. Burnett, and G. Doolen, Phys. Rev. A **15**, 1063 (1977).
[23] W. Müller, J. Flesch, and W. Meyer, J. Chem. Phys. **80**, 3297 (1984).
[24] J. Mitroy, D. C. Griffin, D. W. Norcross, and M. S. Pindzola, Phys. Rev. A **38**, 3339 (1988).
[25] J. Mitroy and M. W. J. Bromley, Phys. Rev. A **68**, 062710 (2003).
[26] M. S. Safronova, A. Derevianko, and W. R. Johnson, Phys. Rev. A **58**, 1016 (1998).
[27] M. S. Safronova, W. R. Johnson, and A. Derevianko, Phys. Rev. A **60**, 4476 (1999).
[28] M. S. Safronova and W. R. Johnson, Adv. At., Mol., Opt. Phys. **55**, 191 (2008).
[29] L. Hamonou and A. Hibbert, J. Phys. B **40**, 3555 (2007).
[30] S. Sahoo, Chem. Phys. Lett. **448**, 144 (2007).
[31] J. Mitroy and M. W. J. Bromley, Phys. Rev. A **68**, 052714 (2003).
[32] J. Mitroy, J. Phys. B **26**, 2201 (1993).
[33] M. W. J. Bromley and J. Mitroy, Phys. Rev. A **65**, 062505 (2002).
[34] J. Mitroy and M. W. J. Bromley, Phys. Rev. A **68**, 035201 (2003).
[35] J. Mitroy, Aust. J. Phys. **52**, 973 (1999).
[36] W. R. Johnson, D. Kolb, and K. Huang, At. Data Nucl. Data Tables **28**, 333 (1983).
[37] S. Hameed, A. Herzenberg, and M. G. James, J. Phys. B **1**, 822 (1968).
[38] S. Hameed, J. Phys. B **5**, 746 (1972).
[39] N. Vaeck, M. Godefroid, and C. Froese Fischer, Phys. Rev. A **46**, 3704 (1992).
[40] G. E. Brown and D. Ravenhall, Proc. R. Soc. London, Ser. A **208**, 552 (1951).
[41] W. R. Johnson, S. A. Blundell, and J. Sapirstein, Phys. Rev. A **37**, 307 (1988).
[42] S. A. Blundell, W. R. Johnson, and J. Sapirstein, Phys. Rev. A **43**, 3407 (1991).
[43] W. R. Johnson, Z. W. Liu, and J. Sapirstein, At. Data Nucl. Data Tables **64**, 279 (1996).
[44] Y. Ralchenko, A. Kramida, J. Reader, and NIST ASD Team, *NIST Atomic Spectra Database Version 3.1.5* (2008) URL http://physics.nist.gov/asd3
[45] U. Volz and H. Schmoranzer, Phys. Scr., T **T65**, 48 (1996).
[46] U. Volz, M. Majerus, H. Liebel, A. Schmitt, and H. Schmoranzer, Phys. Rev. Lett. **76**, 2862 (1996).
[47] E. Tiemann, H. Knockel, and H. Richling, Z. Phys. D: At., Mol. Clusters **37**, 323 (1996).
[48] K. M. Jones, P. S. Julienne, P. D. Lett, W. D. Phillips, E. Tiesinga, and C. J. Williams, Europhys. Lett. **35**, 85 (1996).
[49] C. W. Oates, K. R. Vogel, and J. L. Hall, Phys. Rev. Lett. **76**, 2866 (1996).
[50] W. Ansbacher, Y. Li, and E. H. Pinnington, Phys. Lett. A **139**, 165 (1989).
[51] M. Hermann, V. Batteiger, S. Knunz, G. Saathoff, T. Udem, and T. W. Hansch, e-print arXiv:physics/0808:4061v1.
[52] H. G. Berry, J. Bromander, and R. Buchta, Phys. Scr. **181**, 125 (1970).
[53] J. Kernahan, E. H. Pinnington, J. A. O'Neill, R. L. Brooks, and K. E. Donelly, Phys. Scr. **19**, 267 (1979).
[54] Y. Baudinet-Robinet, P. D. Dumont, H. P. Garnir, E. Biemont, and N. Grevesse, J. Phys. Colloq. **40**, C1 (1979).
[55] S. T. Maniak, E. Träbert, and L. J. Curtis, Phys. Lett. A **173**, 407 (1993).
[56] B. J. Lyons and T. F. Gallagher, Phys. Rev. A **57**, 2426 (1998).
[57] C. E. Theodosiou, L. J. Curtis, and C. A. Nicolaides, Phys. Rev. A **52**, 3677 (1995).
[58] J. Y. Zhang and J. Mitroy, Phys. Rev. A **76**, 022705 (2007).
[59] J. Mitroy, M. W. J. Bromley, and K. G. Rollin (unpublished).
[60] C. Froese Fischer, G. Tachiev, and A. Irimia, At. Data Nucl. Data Tables **92**, 607 (2006).
[61] B. W. Shore and D. H. Menzel, *Principles of Atomic Spectra* (Wiley, New York, 1968).
[62] U. Fano and J. W. Cooper, Rev. Mod. Phys. **40**, 441 (1968).
[63] U. J. Sofia, D. Fabian, and J. C. Howk, Astrophys. J. **531**, 384 (2000).
[64] E. L. Fitzpatrick, Astrophys. J. Lett. **482**, L199 (1997).
[65] S. G. Porsev and A. Derevianko, JETP **129**, 227 (2006).
[66] J. Mitroy and J. Y. Zhang, Phys. Rev. A **76**, 032706 (2007).
[67] J. Mitroy and J. Y. Zhang, Phys. Rev. A **76**, 062703 (2007).
[68] M. S. Safronova, C. J. Williams, and C. W. Clark, Phys. Rev. A **69**, 022509 (2004).
[69] J. Mitroy and M. W. J. Bromley, Phys. Rev. A **70**, 052503 (2004).
[70] R. J. Drachman, Can. J. Phys. **60**, 494 (1982).
[71] A. Kumar and W. J. Meath, Can. J. Chem. **60**, 1616 (1985).
[72] R. R. Freeman and D. Kleppner, Phys. Rev. A **14**, 1614 (1976).
[73] H.-J. Werner and W. Meyer, Phys. Rev. A **13**, 13 (1976).
[74] G. Maroulis and A. J. Thakkar, Chem. Phys. Lett. **156**, 87 (1989).
[75] A. Nicklass, M. Dolg, H. Stoll, and H. Preuss, J. Chem. Phys. **102**, 8942 (1995).
[76] K. Bockasten, Phys. Rev. A **9**, 1087 (1974).
[77] B. Edlen, *Handbuch der Physick* (Springer-Verlag, Berlin, 1964), Vol. 27.
[78] G. W. F. Drake and R. A. Swainson, Phys. Rev. A **44**, 5448 (1991).
[79] R. A. Swainson and G. W. F. Drake, Can. J. Phys. **70**, 187 (1992).
[80] J. Mitroy, Phys. Rev. A **78**, 052515 (2008).
[81] A. Dalgarno and J. T. Lewis, Proc. Phys. Soc., London, Sect. A **69**, 57 (1956).
[82] M. S. Safronova and C. W. Clark, Phys. Rev. A **69**, 040501(R) (2004).